

Warm-Start Variational Quantum Policy Iteration

Nico Meyer^{*,1,2}, Jakob Muraier^{*,1}, Alexander Popov¹, Christian Ufrecht¹
Axel Plinge¹, Christopher Mutschler¹, and Daniel D. Scherer¹

¹Fraunhofer IIS, Fraunhofer Institute for Integrated Circuits IIS, Nürnberg, Germany

²Pattern Recognition Lab, Friedrich-Alexander-Universität Erlangen-Nürnberg, Erlangen, Germany

Abstract—Reinforcement learning is a powerful framework aiming to determine optimal behavior in highly complex decision-making scenarios. This objective can be achieved using policy iteration, which requires to solve a typically large linear system of equations. We propose the variational quantum policy iteration (VarQPI) algorithm, realizing this step with a NISQ-compatible quantum-enhanced subroutine. Its scalability is supported by an analysis of the structure of generic reinforcement learning environments, laying the foundation for potential quantum advantage with utility-scale quantum computers. Furthermore, we introduce the warm-start initialization variant (WS-VarQPI) that significantly reduces resource overhead. The algorithm solves a large FrozenLake environment with an underlying 256×256 -dimensional linear system, indicating its practical robustness.

Index Terms—quantum computing, quantum reinforcement learning, policy iteration, variational quantum algorithms, quantum linear algebra

I. INTRODUCTION.

Quantum reinforcement learning (QRL) [1] is an active field of research at the intersection of quantum computing (QC) and machine learning. The success of classical reinforcement learning (RL) [2], [3] can mostly be attributed to the use of large neural networks as function approximators for the RL setup. The advent of noisy intermediate-scale quantum (NISQ) [4] devices in the last decade has spurred the development of so-called variational approaches [5]. The typical idea in the realm of QRL is to use variational quantum circuits (VQCs) for expressing either the intended behavior directly [6], [7], or approximate an intermediate value function [8], [9]. Extensions include combining multiple function approximators [10], and advanced training routines [11] for the underlying VQCs. While these approaches are quite flexible, they make it difficult to exploit structure of the considered problem, blurring the path to potential quantum advantage.

A more structured approach to RL with dynamic programming is based on so-called policy iteration [12], [13]. However, directly solving the associated large linear system of equations (LSE) is typically intractable with classical methods – requiring to resort to iterative solution methods [14]. This suggests the application of quantum-enhanced linear algebra routines, which provide exponential speed-ups for solving a LSE under certain conditions [15], [16]. Unfortunately, executing those routines requires large-scale fault-tolerant quantum devices,

The research was supported by the Bavarian Ministry of Economic Affairs, Regional Development and Energy with funds from the Hightech Agenda Bayern via the project BayQS.

*These authors contributed equally.

Correspondence to: nico.meyer@iis.fraunhofer.de

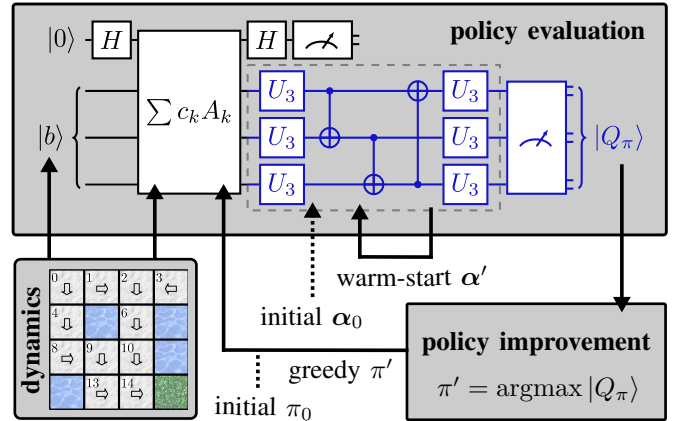


Fig. 1: Proposed routine of variational quantum policy iteration. The evaluation of the state-action value function Q_π is formulated as a LSE $Ax = b$. The solution is computed variationally [17], where the blue sub-circuit prepares a state proportional to Q_π . Classically efficient ℓ_∞ -tomography is used for policy improvement. This procedure is iterated until an optimal policy π_* is found. After random initialization, warm-start variational parameters α are carried over from the previous iteration, leading to faster policy evaluation.

which are currently not available. NISQ-compatible variational algorithms for linear algebra have been proposed [17], [18] – with empirical results suggesting scaling behavior [17] competitive with HHL-based approaches.

Contribution. We introduce the variational quantum policy iteration (VarQPI) algorithm, using a variational linear system solver to perform the quantum-enhanced policy evaluation step within a policy iteration framework. The system matrices associated with generic RL environments are shown to be well-behaved with respect to quantum-enhanced linear algebra routines. We extend the algorithm with a warm-start parameter initialization approach to warm-start VarQPI (WS-VarQPI), which significantly speeds up convergence. The efficiency of the algorithm is demonstrated on different instances of FrozenLake environments, supported with an extensive analysis of the resource requirements.

Related Work. The application of fault-tolerant linear system solvers to quantum policy iteration (QPI) has been studied by Cherrat et al. [19]. We focus our analysis on the NISQ-compatible regime, employing a variational LSE solver proposed in [17] and implemented in the `variational-lse-solver` library [20]. The proposed algorithm uses direct policy evaluation (instead of the typical iterative approach) [13], [14], combined with classically efficient ℓ_∞ tomography [19], [21] for policy improvement.

This work is structured as follows: In Sec. II we introduce preliminaries and describe (warm-start) VarQPI in detail. An experimental demonstration of VarQPI and WS-VarQPI is conducted in Sec. III, completed with experiments on a large FrozenLake environment. An analysis of resource requirements for the quantum-enhanced routine is conducted in Sec. IV. We summarize the results, highlight bottlenecks, and pinpoint potential for future work in Sec. V. We study the LSE induced by typical RL environments regarding requirements on sparseness and condition number in the appendix.

II. PRELIMINARIES AND METHOD DESCRIPTION

RL is an algorithmic framework to solve complex time-dependent decision-making tasks. The underlying Markov Decision Process (MDP) can be expressed as a 5-tuple $(\mathcal{S}, \mathcal{A}, r, p, \gamma)$, with state set \mathcal{S} , and action set \mathcal{A} . The reward function $r(s, a, s') \mapsto \mathbb{R}$ assigns a scalar value to executing action a in state s and transitioning to state s' . The underlying dynamics are described by $p(s'|s, a) \mapsto [0, 1]$, with $\sum_{s'} p(s'|s, a) = 1$ for all $s \in \mathcal{S}$, $a \in \mathcal{A}$. The discount factor $0 \leq \gamma \leq 1$ controls the weighting of immediate and long-term rewards. The goal is to derive a policy $\pi(a|s) \mapsto [0, 1]$, that maximizes the discounted long-term reward $G_t \leftarrow \sum_{t'=t}^{\infty} \gamma^{t'-t} r_{t'}$ over discrete timesteps t , with $r_{t'}$ following the reward function.

A. Direct Policy Iteration

To maximize the long-term reward, one can start off with the Bellman equation for the state-action value function [14]:

$$q_{\pi}(s, a) = \sum_{s'} p(s'|a, s) \left[r(s, a, s') + \gamma \sum_{a'} \pi(a'|s') q_{\pi}(s', a') \right] \quad (1)$$

Solving this equation for a given π is referred to as *policy evaluation*, with existence of a solution being guaranteed for $\gamma < 1$ [14]. Assuming a solution to Eq. (1) for now, one can perform *greedy policy improvement* as

$$\pi(s) \leftarrow \operatorname{argmax}_a q(s, a), \quad (2)$$

with $\pi(a|s) = 1$, if $a = \pi(s)$, and $\pi(a|s) = 0$ otherwise. The repeated execution of policy evaluation and improvement is referred to as *policy iteration*. It is guaranteed to converge to an optimal π_* and typically does so very fast [14].

Evaluating Eq. (1) can be expressed as solving a LSE with $|\mathcal{S}| \cdot |\mathcal{A}|$ equations and unknowns. In practice – due to the large system size – one often resorts to iterative solution methods [14]. Using matrix notation for Eq. (1), we get

$$Q_{\pi} = R + \gamma P \Pi Q_{\pi}, \quad (3)$$

with state-action vector $Q_{\pi} = q(s_i, a_k)_{(ik)} \in \mathbb{R}^{|\mathcal{S}| \times |\mathcal{A}|}$, reward vector $R = \sum_{s'} p(s'|s_i, a_k) r(s_i, a_k, s')_{(ik)} \in \mathbb{R}^{|\mathcal{S}| \times |\mathcal{A}|}$, transition probability matrix $P = p(s'_j | s_i, a_k)_{(ik), j} \in \mathbb{R}^{|\mathcal{S}| \times |\mathcal{A}| \times |\mathcal{S}|}$, and policy matrix $\Pi = \pi(a'_j | s'_j)_{j, (jl)} \in \mathbb{R}^{|\mathcal{S}| \times |\mathcal{S}| \times |\mathcal{A}|}$. Furthermore, Eq. (3) can be re-formulated to

$$(\mathbb{I} - \gamma P \Pi) Q_{\pi} = R, \quad (4)$$

which can be interpreted as a LSE with system matrix $A_{\pi} := \mathbb{I} - \gamma P \Pi$, right-hand side R , and sought-after solution Q_{π} . The generalization of our results to model-free scenarios with function approximation – also referred to as least-squares policy iteration [13] – is left for future work.

B. Variational LSE Solvers

Let the system matrix from Eq. (4) be $A \in \mathbb{R}^{N \times N}$, where $N := |\mathcal{S}| \cdot |\mathcal{A}|$. Classical solution methods scale polynomially in the system size and might become infeasible for large state and action spaces. Quantum-enhanced methods like HHL [15] or modern variants [16], [22] promise poly-logarithmic scaling in the system size N . The use of these techniques in the context of quantum policy iteration has been researched by Cherrat et al. [19]. Unfortunately, executing these algorithms requires large-scale and fault-tolerant quantum devices. An alternative for the NISQ-era is the use of corresponding variational algorithms [23]. While these typically do not provide explicit guarantees of quantum advantage, empirical speed-ups in certain scenarios have been observed. We focus on a variational LSE solver proposed by Bravo-Prieto et al. [17].

In its most abstract form, the algorithm is designed for preparing a state $|x\rangle$, that is proportional to the solution of $Ax = \mathbf{b}$. To enable training, one can use a parameterized ansatz $|x(\alpha)\rangle$. Furthermore, it must be possible to prepare a normalized version of \mathbf{b} , i.e. a state $|b\rangle$. While A is not unitary in general, it is always possible to find a unitary decomposition

$$A = \sum_{k=0}^{L-1} c_k A_k, \quad (5)$$

where c_k are complex coefficients [24] – see also App. C. With the in general not normalized state $|\psi\rangle = A|x(\alpha)\rangle$ and circuit realizations of the unitaries A_k , it is possible to evaluate a loss function

$$C_G = 1 - |\langle b | \Psi \rangle|^2, \quad (6)$$

with $|\Psi\rangle = |\psi\rangle / \langle \psi | \psi \rangle$. The loss vanishes for $|\psi\rangle$ proportional to $|b\rangle$, and therefore can be used to drive the parameters α towards this objective. The use of Hadamard and Hadamard-overlap tests allow the evaluation of the loss function on quantum hardware (see e.g. [17]). Furthermore, Eq. (6) is differentiable, which enables the use of gradient-based optimization techniques. Apart from that, also a local version of the cost function exists, which alleviates training [17]. The routine for VarQPI implemented in this paper is based on the library `variational-lse-solver`, which contains multiple quantum-enhanced LSE solvers [20].

An bound on the required accuracy is given by the operational meaning of the loss function C_G , reading as

$$C_G \geq \frac{\epsilon^2}{\kappa^2} \quad (7)$$

for a desired trace distance ϵ between optimal and approximate solution [17]. Here, $\kappa = \frac{\sigma_{\max}}{\sigma_{\min}}$ denotes the condition number of the system matrix A , where $\sigma_{\max}(A) := \max_{\|x\|=1} \|Ax\|$ and $\sigma_{\min}(A) := \min_{\|x\|=1} \|Ax\|$ denote the largest and smallest

singular values, respectively. We demonstrate in App. B that the systems associated with typical RL environments are well-conditioned. The results in Sec. IV-A suggest that Eq. (7) is not tight, allowing for much faster convergence in practice. Furthermore, matrix sparsity – implicitly assumed throughout the work of Bravo-Prieto et al. [17] – is investigated in App. A.

C. Variational Quantum Policy Iteration with Warm Start

The routine for variational VarQPI combines quantum-enhanced policy evaluation with ℓ_∞ -tomography and classical policy improvement [19], [21] to the following algorithm: For a random initial (deterministic) policy π , one variationally prepares a state $|Q_\pi\rangle \equiv |x(\alpha_*)\rangle$, such that

$$|Q_\pi\rangle \approx \frac{1}{\|Q_\pi\|} \begin{bmatrix} Q_\pi(s=0, a=0) \\ Q_\pi(s=0, a=1) \\ \vdots \\ Q_\pi(s=1, a=0) \\ \vdots \end{bmatrix} \quad (8)$$

$$\sim (\mathbb{I} - \gamma P \Pi)^{-1} R \quad (9)$$

where α_* are the parameters optimized using the algorithm described in Sec. II-B for the system in Eq. (4). Subsequently, multiple preparations of $|Q_\pi\rangle$ are used to acquire counts $M(s, a)$. The raw bitstring measurements are associated with (s, a) following Eq. (8). Policy improvement is furthermore conducted as

$$\pi(s) \leftarrow \operatorname{argmax}_a M(s, a). \quad (10)$$

Since policy iteration converges with respect to the ℓ_∞ norm, it has been shown [19] that $M(s, a)$ can be estimated using ℓ_∞ -tomography (see e.g. [21]). This requires only a polynomial number of samples, even though $M(s, a)$ is of exponential size in the number of qubits.

This application of quantum policy evaluation and classical policy improvement is repeated iteratively. The initial parameters for the first policy evaluation step α_{init}^0 are drawn uniformly at random from $[0, 2\pi]$, and trained to α_*^0 (up to an arbitrary small error threshold). Due to policy iteration updating the value function and associated greedy policy step by step, the greedy actions between successive cycles only change for a limited number of states. Therefore, we assume that $|Q_{\pi^0}\rangle \equiv |x(\alpha_*^0)\rangle$ is reasonably close to $|Q_{\pi^1}\rangle$. Similarly, $|Q_{\pi^i}\rangle$ should be close to $|Q_{\pi^{i+1}}\rangle$ for each two consecutive iterations. Exploiting this, we formulate WS-VarQPI by initializing the variational parameters

$$\alpha_{\text{init}}^{i+1} \leftarrow \alpha_*^i, \quad (11)$$

with α_{init}^0 selected randomly as described above. This procedure is also sketched in Fig. 1. Policy evaluation and improvement is repeated to convergence, i.e. until $\pi^{i+1}(s) = \pi^i(s)$ for all non-terminal states s . We demonstrate in Sec. III-A, that the proposed WS-VarQPI strategy in fact enhances the resource efficiency compared to standard VarQPI, which is consistent with results on warm-start approaches for other types of variational algorithms [25], [26].

Iteration	WS-VarQPI		VarQPI	
	Average Steps	Percentage	Average Steps	Percentage
1	1337 ± 275	100%	1337 ± 275	100%
2	1027 ± 258	100%	1313 ± 295	100%
3	918 ± 262	99%	1497 ± 291	99%
4	690 ± 297	71%	1542 ± 258	70%
5	540 ± 208	29%	1488 ± 223	24%
6	295 ± 40	8%	1578 ± 158	6%

Tab. I: Comparison of required steps for solving the LSE induced by FrozenLake (stochasticity $\beta = 0.1$) with warm-start and random parameter initialization. The values are reported on a per-iteration basis, and averaged over 100 random initial policies. Additionally we report, which percentage of runs has not converged after the indicated iteration number.

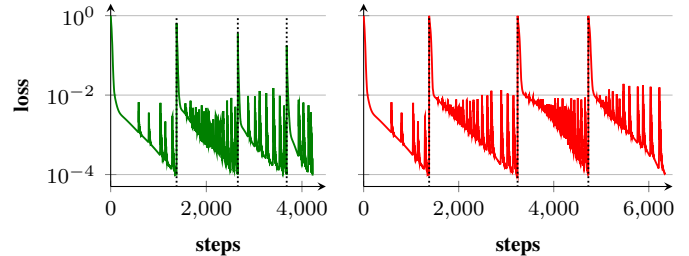


Fig. 2: Loss curves for one instance of WS-VarQPI (left plot) and randomly initialized VarQPI (right plot) on FrozenLake with $\beta = 0.1$. The vertical dotted lines indicate one iteration of policy evaluation with loss threshold 0.0001. The procedure continues with the updated LSE after policy improvement – with the previously optimal parameters, or the initial parameters from the first iteration. The large variance in the training procedure can be attributed to the use of a static learning rate of 0.01. While learning rate schedulers might be used to reduce the fluctuations, the required additional hyperparameter tuning was found to be non-trivial for the proof-of-concept realization.

The improvement regarding time complexity over classical policy iteration depends on the speed-up gained by using the variational LSE solver, which has empirically shown to be super-polynomial under certain conditions [17] – further investigated in Appx. A and B. Furthermore, it is possible to implement an $N \times N$ system using only $\log_2 N$ qubits, providing an exponential improvement w.r.t. space complexity.

III. EXPERIMENTAL END-TO-END REALIZATION

The implementation of the proposed VarQPI and WS-VarQPI algorithms described in Sec. II use the PennyLane-based `variational-lse-solver` library [20]. For depth d , the parameterized ansatz $|x(\alpha)\rangle$ consists of d layers of parameterized U_3 rotations, interleaved by nearest-neighbor CNOT layers, as depicted in Fig. 1 for depth 2. In all experiments we used a learning rate of 0.01 for the Adam optimizer [27] and discount factor $\gamma = 0.9$. These hyperparameters were tuned in order to produce robust convergence for different initial conditions.

For the experiments in this section we resorted to the FrozenLake environment [28], using the standard 4×4 setup shown in Fig. 1. We introduce stochasticity to the environment dynamics by instead transitioning to perpendicular states with probability $0 \leq \beta \leq \frac{1}{3}$. Comparable setups have frequently been considered through the lens of function approximation-based QRL [9], [29]. The 16-state and 4-action

environment induces a 64×64 -dimensional system matrix of the underlying LSE following Eq. (4). With an ancilla qubit for evaluating the loss function with the Hadamard test [17], the realization requires 7 qubits in total. An alternative formulation based on the Hadamard-overlap test [17] requires 13 qubits, but significantly reduces the number of multi-qubit operations. While this is well within the reach of existing NISQ hardware, we resort to classical simulation, due to the limited access to these systems. For the variational quantum policy evaluation routine we constructively decompose the real-valued system matrix A_π into a linear combination of 4 orthogonal matrices [24], [30], satisfying Eq. (5). Details on this procedure and a discussion of potential alternatives are deferred to App. C.

In the following, we report the proof-of-principle realization of the proposed routines, starting out with a comparison of the efficiency of both variants in Sec. III-A. The scalability of the approach is demonstrated in Sec. III-B. An analysis of the resource requirements is deferred to Sec. IV.

A. Warm-Start Parameter Initialization

We compare the performance of the VarQPI algorithm on the `FrozenLake` environment (random parameter initialization in each iteration) to WS-VarQPI (parameter initialization after first iteration as described in Sec. III-A). The circuit depth is $d = 12$, with early-stopping after reaching a loss threshold of 0.0001 – those hyperparameters will be justified in the following section. Averaged over 100 random initial policies for a $\beta = 0.1$ -stochastic `FrozenLake` environment, the warm-start approach converges within 4.1 ± 0.9 iterations, requiring 3943 ± 952 training steps. The randomly-initialized variant requires 4.0 ± 0.9 iterations with 5663 ± 1366 steps. While the negligible difference in iterations can be attributed to statistical variance, the reduction w.r.t. required updates by approx. 30% is clearly significant. From Tab. I it becomes apparent that this difference is more significant in the later iterations. This can be explained by the resulting greedy policy only changing slightly between two successive cycles of policy evaluation and improvement, enhancing the impact of WS-VarQPI. One might expect an even clearer reduction in overall training complexity for larger and more complex environments, where more iterations are required for convergence. We also observed similar results for setups with lower and higher stochasticity.

In Fig. 2 we explicitly report the losses observed during one instance of WS-VarQPI compared to randomly-initialized VarQPI. The warm-start version indeed seems to get initialized to a more desirable part of the optimization landscape, indicated also by the successively reduced initial loss value after policy improvement. For both setups it can be observed, that the loss values start to fluctuate starting from a loss value of about 0.01 – equivalent to the learning rate. This variance can be reduced by using learning rate schedulers, with initial experiments suggesting a linear decay to be best suited. However, this introduces additional hyperparameters, which impede a fair comparison of both routines. While the fluctuations did not hinder the convergence in the considered setups, statements regarding scalability require further investigation.

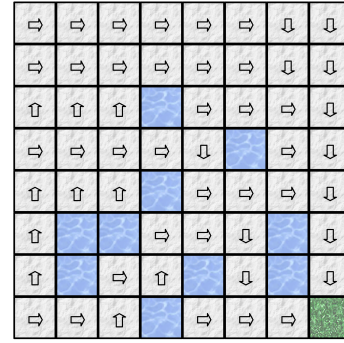


Fig. 3: The policy found for the `FrozenLake8x8` environment with $\beta = 0.1$ -stochasticity using WS-VarQPI. Training required 82160 steps in 9 policy evaluation and improvement cycles. The experiments use a depth $d = 24$ ansatz and a loss threshold of 0.0001. The solution perfectly aligns with the ground truth for this configuration.

B. Up-Scaling to Larger Environment

To strengthen the potential of WS-VarQPI, we execute the algorithm on the $\beta = 0.1$ -stochastic instance of `FrozenLake8x8` in Fig. 3. This 64-state and 4-action setup enlarges the LSE system matrix to a size of 256×256 . This constitutes a 16-fold increase of the matrix size compared to the 4×4 setup. However, the spatial resources for the quantum-enhanced realization only slightly increase from 7 to 9 qubits for the Hadamard formulation, and from 13 to 17 qubits for the Hadamard-overlap formulation.

To additionally account for the larger environment complexity, we increase the circuit depth to $d = 24$, while keeping the loss threshold at 0.0001. Note, however, that this only provides an upper bound on the required resources, and should not be used to infer scaling behavior regarding circuit depth. Within 9 iterations and overall 82160 training steps the learned greedy policy solves the environment. This result was re-produced for 10 random initial policies with only slight deviations in iteration and step number count. While this result does not proof general scalability, it certainly should motivate extending and refining VarQPI and WS-VarQPI.

IV. RESOURCE ANALYSIS OF QUANTUM SUBROUTINE

The spatial resources – i.e. the number of qubits – for variational quantum policy iteration are determined by the size of the system matrix. More concretely, for size $N := |\mathcal{A}| \times |\mathcal{S}|$, the variational ansatz $|x(\alpha)\rangle$ has to act on $n := \lceil \log_2 N \rceil$ qubits. For the training procedure described in Sec. II-B the overall system size scales as $n + 1$ if using the Hadamard test, and as $2n + 1$ if the loss function is evaluated with the Hadamard-overlap test [17].

In the following, we investigate two other crucial components of the overall algorithmic scaling behavior: In Sec. IV-A we demonstrate, that the threshold on the loss function in practice can be selected several orders of magnitude higher than suggested by Eq. (7), allowing for significantly faster convergence. In Sec. IV-B we analyze the depth of the variational ansatz required for reliably solving the linear system.

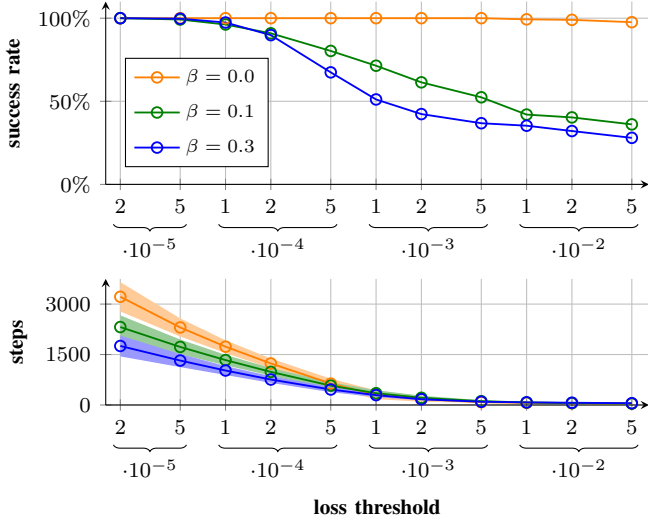


Fig. 4: Success rates of variational quantum policy evaluation with a depth 12 circuit for different loss thresholds and therefore required training steps. The results are averaged over 1000 random instances of `FrozenLake` with varying stochasticity β – the bands in the lower plot denoting standard deviations. Training is terminated once the loss value C_G has declined below the given threshold. The success rate denotes the percentage of runs for which Eq. (10) agrees with the ground truth. To account for sampling noise, we tolerate a deviation of 0.001 in the associated Q -values.

A. Loss Threshold and Environment Stochasticity

As the prepared quantum state $|x(\alpha)\rangle$ is used for greedy policy improvement following Eq. (2), we do not need a perfectly accurate solution to the underlying LSE. It is enough, if the resulting greedy policy aligns with the ground truth – on all non-terminal states. The operational meaning of the loss function from Eq. (7) is proportional to the desired deviation ϵ , and inverse proportional to the condition number κ [17].

We select the tolerated deviation to be 0.001, motivated by the number of shots for approximating $M(s, a)$ being 1000. For the deterministic `FrozenLake` environment the system matrix for a random initial policy has a condition number of 85.6, while the $\beta = 0.3$ -stochastic version exhibits a condition number of 67.4. It is demonstrated in App. B, that the condition numbers for more generic RL environments are in a similar range. Following Eq. (7), the loss thresholds are $C_G \geq \frac{0.001^2}{85.6^2} \approx 1.36 \cdot 10^{-12}$ and $C_G \geq \frac{0.001^2}{67.4^2} \approx 2.20 \cdot 10^{-12}$, respectively. In principle, this should allow for a comparable accuracy with an about 0.6 times lower threshold bound for the stochastic version. However, in practice the deterministic environment is easier to solve, as we will see in the following.

In Fig. 4 we demonstrate, that those bounds are pretty loose for quantum policy iteration, which converges w.r.t. the l_∞ norm. One cycle of quantum policy evaluation and successive policy improvement is successful, if the greedy policy aligns with the ground truth on all non-terminal states. We interpret the overall algorithmic setup to be reliable, if the condition holds for 95% – i.e. two standard deviations – of all random initial policies. Variational quantum policy evaluation works reliably in deterministic `FrozenLake` environments for loss thresholds up to 0.05, improving upon the theoretical bound

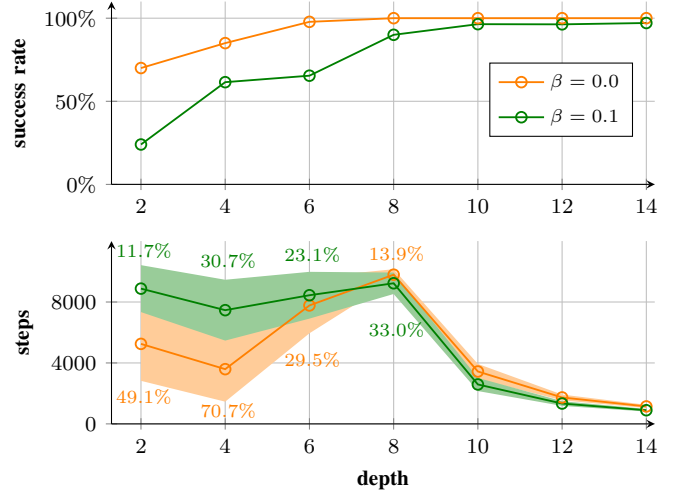


Fig. 5: Success rates of variational quantum policy evaluation for different circuit depths and therefore required training steps. The results are averaged over 1000 random instances of `FrozenLake` with varying stochasticity β – the bands in the lower plot denoting standard deviations. The success rates denotes the percentage of runs for which Eq. (10) agrees with the ground truth. To account for sampling noise, we tolerate a deviation of 0.001 in the associated Q -values. The percentages in the lower plot denote the ration of runs below 100% that achieved the loss threshold 0.0001 with less then 10000 steps, after which training is aborted.

established above by 11 orders of magnitude. For stochastic environments a threshold value of about 0.0001 is required for stable results, still constituting an improvement by about 8 orders of magnitude. It is currently unclear if these practical improvements transfer to the results from App. B, where we considered the general scalability of quantum-enhanced LSE solvers for policy iteration. As indicated in the lower part of Fig. 4, the smaller loss thresholds required for the stochastic environments are partially compensated by a faster convergence compared to deterministic setups.

B. Depth of Variational Ansatz

The depth of the involved circuits mainly depends on two factors: The variational ansatz $|x(\alpha)\rangle$ and the explicit realization of the unitary decomposition following Eq. (5). The latter one can be improved by developing sophisticated matrix decomposition and unitary synthesis tools, which is not part of this work, but is superficially discussed in App. C. The former one will be analyzed in the following.

As before, we select the variational circuit ansatz on n qubits with $d \geq 1$ layers as

$$|x(\alpha)\rangle = \underbrace{U_{\alpha_{d-1}} U_{CX}}_{\text{layer } d-1} \cdots \underbrace{U_{\alpha_1} U_{CX}}_{\text{layer } 1} \underbrace{U_{\alpha_0}}_{\text{layer } 0}, \quad (12)$$

$$\text{with } U_{\alpha_i} = U_3(\alpha_{i,0}) \otimes \cdots \otimes U_3(\alpha_{i,n-1}), \quad (13)$$

$$U_{CX} = CX_{0,1} \cdots CX_{n-2,n-1} CX_{n-1,0}, \quad (14)$$

as also depicted in Fig. 1. In order to determine the actually required number of layers, we report experiments for a varying depth in Fig. 5. Again it becomes apparent that the deterministic `FrozenLake` environment seems to be easier to solve,

as for a given depth the probability that the approximated and ground truth greedy actions align is higher. In general, a more expressive circuit allows for a higher success rate, with reliable accuracy achieved from depth $d = 10$ upwards. Interestingly, this does not consistently hold true for the convergence rate. This measure quantifies the likelihood that the respective ansatz actually allows convergence to the loss threshold 0.0001 in 10000 steps. As indicated in the lower plot, for setups with 8 qubits or less there is no consistent pattern. This can be interpreted as a motivation to investigate ansätze that exploit some structure of the LSE to reduce resource requirements. For deeper circuits this fluctuation disappears with all instances converging. As the required steps for convergence are reduced with increasing circuit depth, we identified $d = 12$ to provide a good balance regarding resource usage.

V. CONCLUSION

In this work we introduced variational quantum policy iteration (VarQPI), an algorithm combining quantum-enhanced policy evaluation with classical policy improvement. It uses a variational LSE solver to perform policy evaluation potentially more efficiently than possible with classical solution methods. The greedy policy improvement step is based on efficient ℓ_∞ -tomography, avoiding the typical bottleneck of exponential sampling complexity for retrieving quantum states.

We demonstrated that the system matrices induced by policy iteration are compatible with requirements imposed by the quantum sub-routines. Specifically, we showed that generic environments satisfy strict sparsity conditions and the associated LSEs are well-conditioned. Both results support the scalability of the approach, which is eminent for potential quantum advantage. One existing bottleneck is the unitary decomposition and synthesis of the matrices, which is left for future work.

The efficiency of the routine was empirically demonstrated on different configurations of the `FrozenLake` environment. We discovered that a version with warm-start parameter initialization (WS-VarQPI) can significantly improve the convergence behavior. We conducted an analysis of different hyperparameters settings to support the robustness of the approach.

We are confident that (WS-)VarQPI opens the way for a promising line of research on noisy intermediate-scale quantum (NISQ)-compatible quantum reinforcement learning. The successful application to a complex `FrozenLake8x8` environment underlines the potential of the approach. Future research could include the extension to model-free scenarios and validation experiments on quantum hardware.

CODE AVAILABILITY

An implementation of VarQPI and WS-VarQPI, including the considered environments, is available in the repository <https://github.com/nicomeyer96/ws-varqpi>. Usage details and instructions on how to reproduce the main results of this paper can be found on the `README` file. Further information and data is available upon reasonable request.

APPENDIX

Both fault-tolerant and NISQ-compatible linear system of equations (LSE) solvers promise speed-ups only under certain restrictions. Two conditions are sparsity and low condition number of the system matrix A [19], [31]. While the former is not explicitly stated in the error bounds of the variational LSE solver, the scaling and matrix decomposition results implicitly assume sparsity [17]. We demonstrate in the following, that the linear systems associated with typical reinforcement learning (RL) setups are well-behaved regarding these conditions.

A. Sparsity for Local Dynamics

Quantum linear system solvers assume sparsity of the $N \times N$ system matrix A , with only $\mathcal{O}(N \cdot \text{polylog}(N))$ non-zero entries [17], [31]. A stronger assumption is that each of the N rows of A has at most $\mathcal{O}(\text{polylog}(N))$ non-zero elements.

For state set \mathcal{S} , action set \mathcal{A} , and dynamics p , we define the set of states that can be reached from s under action a as

$$\mathcal{S}_{s,a} = \{s' \mid p(s'|s,a) > 0\}, \quad (15)$$

and the set of states that can transition to s' under action a as

$$\bar{\mathcal{S}}_{s',a} = \{s \mid p(s'|s,a) > 0\}. \quad (16)$$

Definition 1 (local dynamics). *An environment with state set \mathcal{S} and action set \mathcal{A} has local dynamics, if it holds*

$$|\mathcal{S}_{s,a}| \leq \log_2(N), \quad (17)$$

$$|\bar{\mathcal{S}}_{s',a}| \leq \log_2(N) \quad (18)$$

for all $s, s' \in \mathcal{S}$, $a \in \mathcal{A}$, with $N := |\mathcal{S}|$.

These assumptions are reasonable in the context of RL, as transition probabilities typically decrease with (spatial) distance between states. As in quantum policy iteration (QPI) the policy is deterministic, the policy matrix defined in Eq. (3) has exactly one non-zero entry in each row. Consequently, $P_\pi = P\Pi$ is row-stochastic with at most $\log_2(N)$ non-zero entries per row and column for Def. 1. The system matrix $A_\pi = \mathbb{I} - \gamma P_\pi$ contains at most one additional non-zero element in each row, not changing the overall scaling. Therefore, locally-dynamic environments satisfy the sparsity condition posed by quantum-enhanced LSE solvers stated above. Additionally, this guaranteed sparsity is a desirable property for allowing an efficient unitary decomposition of A_π , as further elaborated in App. C.

Depending on the concrete dynamics function p , one can consider special cases of environments satisfying Def. 1:

Definition 2 (deterministic dynamics). *An environment with state set \mathcal{S} and action set \mathcal{A} has deterministic dynamics, if*

$$|\mathcal{S}_{s,a}| = 1, \quad (19)$$

$$|\bar{\mathcal{S}}_{s',a}| \leq \log_2(N) \quad (20)$$

for all $s, s' \in \mathcal{S}$, and $a \in \mathcal{A}$. Consequently, for all $s \in \mathcal{S}$, $a \in \mathcal{A}$ there is only one $s' \in \mathcal{S}$ such that

$$p(s'|s,a) = 1, \quad (21)$$

while for all other $s' \in \mathcal{S}$ it holds $p(s'|s,a) = 0$.

Definition 3 (uniform local dynamics). *An environment with state set \mathcal{S} and action set \mathcal{A} has uniform local dynamics, if*

$$|\mathcal{S}_{s,a}| = \log_2(N), \quad (22)$$

$$|\bar{\mathcal{S}}_{s',a}| \leq \log_2(N) \quad (23)$$

for all $s, s' \in \mathcal{S}$, $a \in \mathcal{A}$, with $N = |\mathcal{S}|$. Furthermore, for all $s \in \mathcal{S}$, $a \in \mathcal{A}$ there are $\log_2(N)$ different $s' \in \mathcal{S}$ such that

$$p(s'|s, a) = \frac{1}{\log_2(N)}, \quad (24)$$

while for all other $s' \in \mathcal{S}$ it holds $p(s'|s, a) = 0$.

Definition 4 (exponential local dynamics). *An environment with state set \mathcal{S} and action set \mathcal{A} has exponential local dynamics, if*

$$|\mathcal{S}_{s,a}| = \log_2(N), \quad (25)$$

$$|\bar{\mathcal{S}}_{s',a}| \leq \log_2(N) \quad (26)$$

for all $s \in \mathcal{S}$, $a \in \mathcal{A}$, with $N = |\mathcal{S}|$. Furthermore, for all $s \in \mathcal{S}$, $a \in \mathcal{A}$ there are $\log_2(N)$ different $s' \in \mathcal{S}$ such that

$$p(s'|s, a) = \frac{\exp((1 - 1/\beta)d(s, s'))}{\sum_{s'' \in \mathcal{S}_{s,a}} \exp((1 - 1/\beta)d(s, s''))}, \quad (27)$$

with perturbation parameter $\beta \in (0, 1]$ and some distance measure $d: \mathcal{S} \times \mathcal{S} \mapsto \mathbb{R}_+$, while for all other $s' \in \mathcal{S}$ it holds $p(s'|s, a) = 0$.

The *exponential local dynamics* in Def. 4 assume, that the transition probabilities vanish exponentially within a logarithmic local neighborhood. The *deterministic dynamics* in Def. 2 are a special case with $\beta \rightarrow 0$. Furthermore, the *uniform local dynamics* from Def. 3 describe the opposite extreme with $\beta = 1$. While all environments with dynamics following Defs. 1 to 4 satisfy the imposed sparsity constraints, guarantees w.r.t. the condition number vary, as will be discussed in the following.

B. Bounds on Condition Number

Quantum-enhanced LSE solvers require a small condition number $\kappa = \frac{\sigma_{\max}}{\sigma_{\min}}$ of the system matrix A_π [19], [31], where σ_{\max} and σ_{\min} denote the largest and smallest singular values, respectively. This can be seen in the threshold bounds from Eq. (7), where κ enters in the denominator. We demonstrate that the LSE associated with typical RL setups are well-conditioned, supporting the feasibility of larger-scale QPI.

We need to mention, that the analytical bound to the condition number derived in Cherrat et al. [19] does not hold for generic RL setups. The authors state, that for $A_\pi := \mathbb{I} - \gamma P_\pi$ the condition number $\kappa(A_\pi)$ is upper-bounded by $\frac{1+\gamma}{1-\gamma}$ (see Theorem 7 of [19]). However, the proof assumes that $\|P_\pi\| = 1$, which only holds for doubly-stochastic P_π [32]. The matrices P_π of typical Markov Decision Processes (MDPs) in general are only row-stochastic, not allowing this assumption.

In the following, we derive corrected bounds for the general setup, empirically show that the systems are well-conditioned, and re-discover the bounds stated by Cherrat et al. for a special case. Therefore, we first state and prove some helpful properties of matrix norms:

Proposition 1. *For a square matrix $A \in \mathbb{C}^{N \times N}$ it holds*

$$\|A^{-1}\|_\infty \leq \frac{1}{\min_i\{|A_{ii}| - \sum_{i \neq j} |A_{ij}|\}}, \quad (28)$$

assuming the denominator on the right side is positive.

Proof. Let us define $w = Av$, with column vectors $v, w \in \mathbb{C}^N$. By following the definition of an arbitrary operator norm as $\|A\| = \sup\{\|Av\| : \|v\| = 1\}$ we need to show

$$\|w\|_\infty \leq 1 \Rightarrow \|v\|_\infty \leq \frac{1}{\min_i\{|A_{ii}| - \sum_{i \neq j} |A_{ij}|\}} \quad (29)$$

$$\Leftrightarrow \|w\|_\infty \leq \min_i\{|A_{ii}| - \sum_{i \neq j} |A_{ij}|\} \Rightarrow \|v\|_\infty \leq 1, \quad (30)$$

with a stronger statement reading as

$$\forall i, j : |w_i| \leq |A_{ii}| - \sum_{i \neq j} |A_{ij}| \Rightarrow \forall i : |v_i| \leq 1. \quad (31)$$

Let us assume the contrary, i.e. it exists an index i , such that $|v_i| > 1$. Then it holds

$$|w_i| = |A_{ii}v_i - \sum_{i \neq j} A_{ij}(-v_j)| \quad (32)$$

$$\geq |A_{ii}||v_i| - \sum_{i \neq j} |A_{ij}||v_j| \quad (33)$$

$$> |A_{ii}| - \sum_{i \neq j} |A_{ik}|, \quad (34)$$

contradicting the condition from Eq. (31), and thereby proving the original statement by contraposition. \square

Proposition 2. *For a square matrix $A \in \mathbb{C}^{N \times N}$ it holds*

$$\|A^{-1}\|_1 \leq \frac{1}{\min_i\{|A_{ii}| - \sum_{i \neq j} |A_{ji}|\}}, \quad (35)$$

assuming the denominator on the right side is positive.

Proof. Let us define $w = vA$, with row vectors $v, w \in \mathbb{C}^N$. The proof is equivalent to the proof of Prop. 1. \square

We prove an upper bound to the condition number of environments with general local dynamics:

Theorem 1. *Let $A_\pi := \mathbb{I} - \gamma P_\pi$ be the $N \times N$ -dimensional system matrix of a LSE with underlying local dynamics following Def. 1. The condition number of the matrix is upper bounded by*

$$\kappa(A_\pi) \leq \sqrt{N + \gamma \cdot N \log_2(N)} \cdot \frac{\sqrt{1 + \gamma}}{1 - \gamma}. \quad (36)$$

Proof. We first show an upper bound to the largest singular value, using Hölder's inequality:

$$\sigma_{\max}(A_\pi) \leq \sqrt{\|A_\pi\|_\infty} \sqrt{\|A_\pi\|_1} \quad (37)$$

$$\leq \sqrt{1 + \gamma} \sqrt{1 + \gamma \cdot \log_2(N)} \quad (38)$$

The bound for the maximum row sum follows directly from the row-stochasticity of P_π , while the bound for the maximum column sum additionally employs the logarithmically restricted locality of the dynamics underlying P_π .

Next, we show a lower bound to the smallest singular value, using the Cauchy-Schwarz inequality and Prop. 1:

$$\sigma_{\min}(A_{\pi}) = \frac{1}{\|A_{\pi}^{-1}\|} \geq \frac{1}{\sqrt{N}\|A_{\pi}^{-1}\|_{\infty}} \quad (39)$$

$$\geq \frac{1}{\sqrt{N} \frac{1}{1-\gamma}} \quad (40)$$

Plugging these results into the definition of the condition number reveals the stated bound. \square

Assuming environments with uniform local dynamics, it is possible to derive a much tighter bound:

Theorem 2. *Let $A_{\pi} := \mathbb{I} - \gamma P_{\pi}$ be the $N \times N$ -dimensional system matrix of a LSE with underlying uniform local dynamics following Def. 3. The condition number of the matrix is upper bounded by*

$$\kappa(A_{\pi}) \leq \frac{1+\gamma}{1-\gamma}. \quad (41)$$

Proof. We first show an upper bound to the largest singular value, using Hölder's inequality:

$$\sigma_{\max}(A_{\pi}) \leq \sqrt{\|A_{\pi}\|_{\infty}} \sqrt{\|A_{\pi}\|_1} \quad (42)$$

$$\leq \sqrt{1+\gamma} \sqrt{1+\gamma} \quad (43)$$

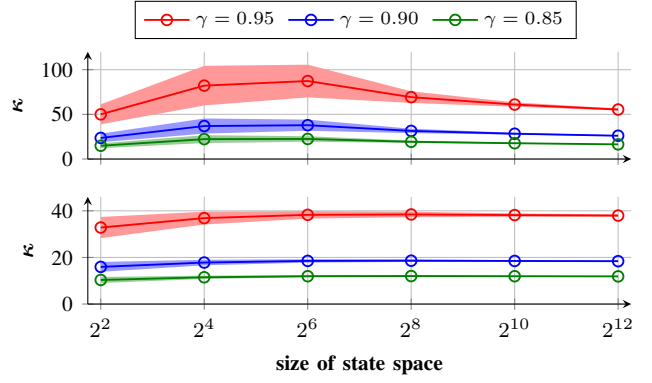
The bound for the maximum row sum follows directly from the row-stochasticity of P_{π} , while the bound for the maximum column sum additionally employs the logarithmically restricted locality of the dynamics underlying P_{π} , and the maximum sum of non-diagonal column entries being $\gamma \cdot \log_2(N) \cdot \frac{1}{\log_2 N}$. Next, we show a lower bound to the smallest singular value, using Hölder's inequality and Props. 1 and 2:

$$\sigma_{\min}(A_{\pi}) = \frac{1}{\|A_{\pi}^{-1}\|} \geq \frac{1}{\sqrt{\|A_{\pi}^{-1}\|_{\infty}} \sqrt{\|A_{\pi}^{-1}\|_1}} \quad (44)$$

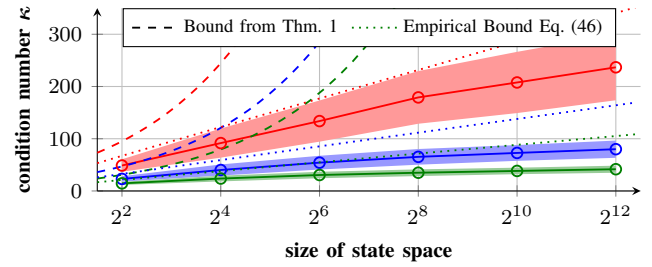
$$\geq \frac{1}{\sqrt{\frac{1}{1-\gamma}} \sqrt{\frac{1}{1-\gamma}}} \quad (45)$$

The bound for the maximum row sum follows directly from the row-stochasticity of P_{π} , while the bound for the maximum column sum exploits the uniform locality as described above. Plugging these results into the definition of the condition number reveals the stated bound. \square

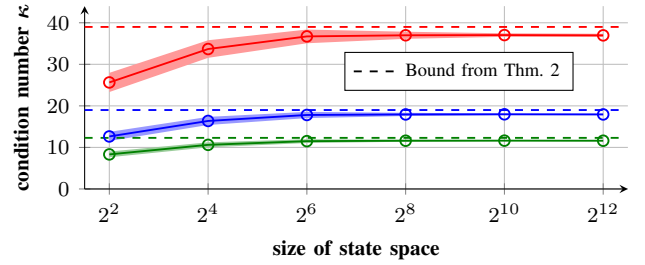
Interestingly, when assuming uniform locality the bound from Thm. 2 is independent of the system size N and only scales with the discount parameter γ . On the contrary, the bound for general local dynamics stated in Thm. 1 scales as $\mathcal{O}(\sqrt{N \log N})$, assuming γ is close to one – which it usually is in practical setups. As N scales in the qubit number as $N = 2^n$, this bound exhibits an exponential scaling. We assume it is possible to derive tighter bounds also for the general case, by incorporating statistical arguments. This might allow for applying Prop. 2 for bounding the smallest singular value in the proof of Thm. 1. However, such considerations are out of the scope of this work.



(a) Environments with $\beta = 0.1$ (upper plot) and $\beta = 0.4$ (lower plot) exponential local dynamics following Def. 4.



(b) Environment with deterministic dynamics following Def. 2.



(c) Environment with uniform local dynamics following Def. 3.

Fig. 6: Condition number averaged over 100 random LSEs with underlying local dynamics. Environments with exponential local dynamics are considered in (a), with a clear convergence of the condition number. The special case of deterministic dynamics is considered in (b), with the bound obtained from Thm. 1 being extremely loose. From the data one can assume the statistical upper bound in Eq. (46). The instances with uniform local dynamics in (c) are well-conditioned for arbitrary system size as follows from Thm. 2.

We summarize the results of empirically evaluating the condition number for different environment dynamics in Fig. 6. For local dynamics the systems are well-conditioned, as shown in Fig. 6(a). The loose bounds for deterministic dynamics suggest, that the estimate in Eq. (39) can be tightened from \sqrt{N} to $\sqrt{\log_2(N)}$, resulting in the upper bound

$$\sqrt{\log_2(N) + \gamma \log_2^2(N)} \cdot \frac{\sqrt{1+\gamma}}{1-\gamma}. \quad (46)$$

This scaling behavior of $\mathcal{O}(\log N)$ aligns with the results in Fig. 6(b). We therefore suggest it is reasonable to assume, that κ grows at most (sub-)linearly with the number of qubit – i.e. logarithmically in the system size. For the local uniform

dynamics in Fig. 6(c), the bound given in Thm. 2 is shown to be tight. As it is independent of the system size, there are no principled roadblocks regarding scalability. The in-between cases in Fig. 6(a) are guaranteed the upper bound from Thm. 1, but with increasing value of β seem to approach the bounds of Thm. 2. Moreover, the dependence of the loss threshold on the condition number is limited, as observed in Sec. IV-A.

C. Notes on Unitary Decomposition

Executing the variational LSE solver from Sec. II-B on quantum hardware requires access to a unitary decomposition following Eq. (5). For our proof-of-concept experiments we made use of the fact that all real matrices can be decomposed into an affine combination $A/\|A\| = X + X^t + Y - Z$, with X, Y, Z unitary [24], [30]. It has to be noted, that explicitly determining the decomposition requires performing a singular value decomposition (SVD). Consequently, using a classical SVD technique for this construction would be an bottleneck canceling out potential quantum advantage of variational policy iteration. For hardware realizations one also needs to consider the complexity of unitary synthesis [33], which this work factored out by simulating full unitaries using the `variational-lse-solver` library [20].

Closer examining and eliminating this bottleneck is out of the scope of this paper. However, it has already been shown, that quantum access is possible to the LSE underlying specific RL environments [19]. A promising tool might also be the use of Szegedy walks, which are especially suited for sparse systems [34], [35]. Trading a larger number of decomposition terms for a trivial unitary synthesis, one might also consider tree-based approaches for Pauli decomposition [36].

REFERENCES

- [1] N. Meyer, C. Ufrecht, M. Periyasamy, D. D. Scherer, A. Plinge, and C. Mutschler, "A Survey on Quantum Reinforcement Learning," *arXiv:2211.03464*, 2022.
- [2] J. Jumper, R. Evans, A. Pritzel, T. Green, M. Figurnov, O. Ronneberger, K. Tunyasuvunakool, R. Bates, A. Židek, A. Potapenko *et al.*, "Highly accurate protein structure prediction with AlphaFold," *Nature*, vol. 596, no. 7873, pp. 583–589, 2021.
- [3] F. J. Ruiz, T. Laakkonen, J. Bausch, M. Balog, M. Barekatin, F. J. Heras, A. Novikov, N. Fitzpatrick, B. Romera-Paredes, J. van de Wetering *et al.*, "Quantum Circuit Optimization with AlphaTensor," *arXiv:2402.14396*, 2024.
- [4] J. Preskill, "Quantum computing in the NISQ era and beyond," *Quantum*, vol. 2, p. 79, 2018.
- [5] K. Bharti, A. Cervera-Lierta, T. H. Kyaw, T. Haug, S. Alperin-Lea, A. Anand, M. Degroote, H. Heimonen, J. S. Kottmann, T. Menke *et al.*, "Noisy intermediate-scale quantum algorithms," *Rev. Mod. Phys.*, vol. 94, no. 1, p. 015004, 2022.
- [6] S. Jerbi, C. Gyurik, S. Marshall, H. Briegel, and V. Dunjko, "Parametrized Quantum Policies for Reinforcement Learning," *Adv. Neural Inf. Process. Syst.*, vol. 34, pp. 28 362–28 375, 2021.
- [7] N. Meyer, D. Scherer, A. Plinge, C. Mutschler, and M. Hartmann, "Quantum Policy Gradient Algorithm with Optimized Action Decoding," in *International Conference on Machine Learning (ICML)*, vol. 202. PMLR, 2023, pp. 24 592–24 613.
- [8] S. Y.-C. Chen, C.-H. H. Yang, J. Qi, P.-Y. Chen, X. Ma, and H.-S. Goan, "Variational Quantum Circuits for Deep Reinforcement Learning," *IEEE Access*, vol. 8, pp. 141 007–141 024, 2020.
- [9] A. Skolik, S. Jerbi, and V. Dunjko, "Quantum agents in the Gym: a variational quantum algorithm for deep Q-learning," *Quantum*, vol. 6, p. 720, 2022.
- [10] S. Wu, S. Jin, D. Wen, and X. Wang, "Quantum reinforcement learning in continuous action space," *arXiv:2012.10711*, 2023.
- [11] N. Meyer, D. D. Scherer, A. Plinge, C. Mutschler, and M. J. Hartmann, "Quantum Natural Policy Gradients: Towards Sample-Efficient Reinforcement Learning," in *IEEE International Conference on Quantum Computing and Engineering (QCE)*, vol. 2, 2023, pp. 36–41.
- [12] R. A. Howard, *Dynamic programming and markov processes*. John Wiley, 1960.
- [13] M. G. Lagoudakis and R. Parr, "Least-squares policy iteration," *J. Mach. Learn. Res.*, vol. 4, pp. 1107–1149, 2003.
- [14] R. S. Sutton and A. G. Barto, *Reinforcement Learning: An Introduction*. The MIT Press, 2018.
- [15] A. W. Harrow, A. Hassidim, and S. Lloyd, "Quantum Algorithm for Linear Systems of Equations," *Phys. Rev. Lett.*, vol. 103, no. 15, p. 150502, 2009.
- [16] G. H. Low and I. L. Chuang, "Hamiltonian Simulation by Qubitization," *Quantum*, vol. 3, p. 163, 2019.
- [17] C. Bravo-Prieto, R. LaRose, M. Cerezo, Y. Subasi, L. Cincio, and P. J. Coles, "Variational quantum linear solver," *Quantum*, vol. 7, p. 1188, 2023.
- [18] X. Xu, J. Sun, S. Endo, Y. Li, S. C. Benjamin, and X. Yuan, "Variational algorithms for linear algebra," *Science Bulletin*, vol. 66, no. 21, pp. 2181–2188, 2021.
- [19] E. A. Cherratt, I. Kerenidis, and A. Prakash, "Quantum reinforcement learning via policy iteration," *Quantum Mach. Intell.*, vol. 5, no. 2, p. 30, 2023.
- [20] N. Meyer, M. Röhn, J. Murauer, D. D. Scherer, A. Plinge, and C. Mutschler, "Comprehensive Library of Variational LSE Solvers," *arXiv:2404.09916*, 2024.
- [21] I. Kerenidis, J. Landman, and A. Prakash, "Quantum algorithms for deep convolutional neural networks," *arXiv:1911.01117*, 2019.
- [22] A. Gilyén, Y. Su, G. H. Low, and N. Wiebe, "Quantum singular value transformation and beyond: exponential improvements for quantum matrix arithmetics," in *Proceedings of the 51st Annual ACM SIGACT Symposium on Theory of Computing*, 2019, pp. 193–204.
- [23] M. Cerezo, A. Arrasmith, R. Babbush, S. C. Benjamin, S. Endo, K. Fujii, J. R. McClean, K. Mitarai, X. Yuan, L. Cincio *et al.*, "Variational quantum algorithms," *Nat. Rev. Phys.*, vol. 3, no. 9, pp. 625–644, 2021.
- [24] X. Zhan, "Span of the orthogonal orbit of real matrices," *Linear and Multilinear Algebra*, vol. 49, no. 4, pp. 337–346, 2001.
- [25] Y.-F. Niu, S. Zhang, and W.-S. Bao, "Warm starting variational quantum algorithms with near clifford circuits," *Electronics*, vol. 12, no. 2, p. 347, 2023.
- [26] F. Truger, J. Barzen, F. Leymann, and J. Obst, "Warm-starting the vqe with approximate complex amplitude encoding," *arXiv:2402.17378*, 2024.
- [27] D. P. Kingma and J. Ba, "Adam: A method for stochastic optimization," *arXiv:1412.6980*, 2014.
- [28] G. Brockman, V. Cheung, L. Pettersson, J. Schneider, J. Schulman, J. Tang, and W. Zaremba, "OpenAI Gym," *arXiv:1606.01540*, 2016.
- [29] T.-A. Drăgan, M. Monnet, C. B. Mendl, and J. M. Lorenz, "Quantum Reinforcement Learning for Solving a Stochastic Frozen Lake Environment and the Impact of Quantum Architecture Choices," *arXiv:2212.07932*, 2022.
- [30] C.-K. Li and E. Poon, "Additive decomposition of real matrices," *Linear and Multilinear Algebra*, vol. 50, no. 4, pp. 321–326, 2002.
- [31] A. M. Childs, R. Kothari, and R. D. Somma, "Quantum algorithm for systems of linear equations with exponentially improved dependence on precision," *SIAM Journal on Computing*, vol. 46, no. 6, pp. 1920–1950, 2017.
- [32] R. A. Horn and C. R. Johnson, *Matrix analysis*. Cambridge university press, 2012.
- [33] S. Rietsch, A. Y. Dubey, C. Ufrecht, M. Periyasamy, A. Plinge, C. Mutschler, and D. D. Scherer, "Unitary synthesis of clifford+ t circuits with reinforcement learning," *arXiv:2404.14865*, 2024.
- [34] Y. Subasi, R. D. Somma, and D. Orsucci, "Quantum algorithms for systems of linear equations inspired by adiabatic quantum computing," *Phys. Rev. Lett.*, vol. 122, no. 6, p. 060504, 2019.
- [35] M. Szegedy, "Quantum speed-up of Markov chain based algorithms," in *45th Annual IEEE symposium on foundations of computer science*, 2004, pp. 32–41.
- [36] O. Koska, M. Baboulin, and A. Gazda, "A tree-approach Pauli decomposition algorithm with application to quantum computing," *arXiv:2403.11644*, 2024.